DIRECT NUMERICAL SIMULATION OF NON-CHANNELIZED PARTICLE-LADEN GRAVITY CURRENTS

Ezequiel P. Francisco, ezequiel.francisco@acad.pucrs.br
L. F. Espath, espath@gmail.com
J. H. Silvestrini, jorgehs@pucrs.br
Faculdade de Engenharia, Pontifícia Universidade Católica do Rio Grande do Sul - PUCRS

S. Laizet, s.laizet@imperial.ac.uk
Imperial College London - UK

Abstract. *We present here high-fidelity simulations of particle-laden gravity currents for a non-channelized non-axisymmetric configuration. Results of previous works based on experimental and numerical studies for axissymetric configurations are used to stablish comparisons. The focus of this investigation is understand how the Reynolds number and how the dimensions of the reservoir of the mixture particle-fluid affect the dynamics of the current when it is spreading over a flat bed. The results show that the higher Reynolds number contributes for the lateral spreading whereas the narrower reservoir is important for the longitudinal spreading. The deposit map indicates an uniform distribution of particle over the bottom for the simulations with a wider channel.*

Keywords: *Particle-laden gravity currents, direct numerical simulation, non-channelized, non-axissymetric.*

1. INTRODUCTION

Particle-laden gravity currents are flows in which the driving force is supplied by density differences caused by the presence of suspended particles. When the current is denser than surrounding fluid, it will propagate below the surrounding fluid (Ungarish, 2006) due to a horizontal pressure gradient created by the gravitational force acting on the density excess (Cantero et al., 2007a). It is observed in this kind of flow the development of highly complex turbulent structures, such as the lobe-and-cleft patterns at the current frontal portion, and the Kelvin-Helmholtz vortices in the interface between the current and the fresh fluid. The occurrence of gravity currents in the nature is associated with the movement of cold and warm air masses which give rise to the storms, sand storms, movement of oceanic currents due to the difference in saline and/or temperature concentrations and the avalanches, for example.

Submarine currents are the most important mechanism for transporting sediments to deeper regions of the oceans. The deposits originated from such currents provide valuable informations about the geological history of the Earth as well as they can give rise to hydrocarbon reservoirs where oil and gas are found (Kneller and Buckee, 2000). Depending on the magnitude, gravity currents are able to destroy seafloor equipments like pipes and communication cables (Meiburg and Kneller, 2010).

The above pointed is the great importance for the geological and engineering contexts, so that the correct understanding of the governing physical mechanisms of the gravity currents able us to make predictions about their main features. Researches are been reported in the last thirty years trying to establish models to predict the front evolution and the sedimentation process, for example. The observation *in situ* of an event is difficult because its unpredictability. The most commonly used ways to study them are the laboratory experiments and numerical simulations in a channelized configuration, well known as lock-exchange. In this configuration a mixture of fresh fluid and particles, uniformly suspended, is initially locked in a reservoir separated from the fresh fluid by a gate. After removing the gate, the denser fluid horizontally propagates constrained by the channel walls in the spanwise direction. The work of Rooij and Dalziel (2001) presents a description of the deposit profile for a mono-disperse flow, i.e., a flow where the suspension is formed by particles with the same diameter. Blanchette et al. (2006) and Gray et al. (2005) perform a case including a complex geometry in bottom of the domain. Necker et al. (2002), Necker et al. (2005), Espath et al. (2014) and Espath et al. (2015) evaluate the energy balance of the gravity currents in order to find the relation between potential and kinetic energy with dissipative terms.

Recently, several authors have been presented works in a non-channelized configuration with cylindrical or rounded rectangle as initial reservoirs. Numerical simulations were made by Cantero (2006; 2007b) to study the dynamics of a non-channelized current with axisymmetric initial reservoir as well as how the Reynolds number impacts in the main structures of the flow. Zgheib et al. (2015a; 2015b; 2015c) used numerical simulations and laboratory experiments, in a non-channelized configuration whit cylindrical and non-axisymmetric initial reservoir, to establish prediction models for the spreading of the currents.

The present work aims to use Direct Numerical Simulation (DNS) in a non-channelized non-axisymmetric configuration in order to understand the dynamics of the current spreading and what is the importance of the Reynold number and the aspect ratio of the initial reservoir for the current time evolution and sedimentation process by means qualitative and quantitative analysis.

2. CONFIGURATION AND GOVERNING EQUATIONS

The performed Direct Numerical Simulations are based on the channel-basin lock-exchange configuration as shown in Fig. 1. This set-up consists on an initial sub-volume of $L_{1_s} \times L_{2_s} \times L_{3_s}$ dimensions, filled with a mixture of particles and fresh fluid. Initially the sub-volume is separated from the rest of the domain by a virtual lock gate. After remove the gate, an underflow begins spreading in the positive x_1 and lateral x_3 directions, differently of the axisymmetric configuration studied by Zgheib et al. (2015a; 2015b; 2015c) which the flow spreads in all directions.

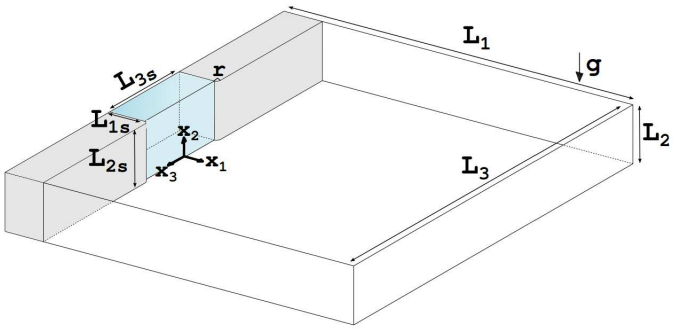

Figure 1: Initial set-up of the channel-basin lock-exchange problem. The computational domain has length L_1, height L_2 and width L_3. Note that the channel-basin transition is rounded with a radius $r = 0.2$.

We assume a low initial volume fraction of suspended particles, not more than 1%, what allows to neglect the inertial interaction among the particles and leading us to an approach of diluted mixture. Despite we do not simulate each single particle, its interaction with the flow is characterized by the momentum and mass exchange. Such diluted approach results in a very small density difference between the current and the surrounding fresh fluid, simplifying our equations for the incompressible flows under Boussinesq assumption. The particle fraction is characterized by the particle terminal fall velocity, well known as settling velocity u^s and it is obtained by the Stokes settling velocity law, closely agreeing with small particle diameters ($d_p < 0.1mm$) (Julien, 2010). Using this law we assume that the Stokes drag force is the dominant force acting over spherical particles. However Gladstone et al. (1998) suggest u^s values one third smaller for the results of the Stokes settling velocity law because natural particles usually are not spherical.

To numerically solve this kind of flow we employ the incompressible Navier-Stokes equations and use the half of the domain height ($\tilde{h} = \tilde{L}_2/2$) and the buoyancy velocity ($\tilde{u}_b$) as the characteristic length and velocity scales. Here, the tilde represents a dimensional quantity. The buoyancy velocity is defined as

$$\tilde{u}_b = \sqrt{\tilde{g}\frac{(\tilde{\rho}_p - \tilde{\rho}_0)}{\tilde{\rho}_0} C_r \tilde{h}}, \tag{1}$$

where $\tilde{g}(\tilde{\rho}_p - \tilde{\rho}_0)C_r/\tilde{\rho}_0$ is the reduced gravitational acceleration g'. The particle and ambient fluid densities are $\tilde{\rho_p}$ and $\tilde{\rho_0}$, respectively. $\tilde{g}$ is the gravitational acceleration whereas C_r is the total initial volume fraction of particles in the sub-volume and it is taken as a characteristic parameter as well. Thus, the dimensionless incompressible Navier-Stokes equations can be written as

$$\frac{\partial u_i}{\partial x_i} = 0, \tag{2}$$

$$\frac{\partial u_i}{\partial t} + u_j \frac{\partial u_i}{\partial x_j} = -\frac{\partial p}{\partial x_i} + \frac{1}{Re}\frac{\partial^2 u_i}{\partial x_j \partial x_j} + ce^g. \tag{3}$$

In the above equations, $e^g = (0, -1, 0)$ is the unit vector acting in gravity direction, as well as u_i, p and c represent the velocity field, pressure and particle concentration, respectively. Here appears the Reynolds number which is defined as $Re = (\tilde{u}_b\tilde{h})/\tilde{\nu}$, where $\tilde{\nu}$ denotes de kinematic viscosity of the fluid. In order to describe the concentration field of the domain, the following advection-diffusion equation is employed

$$\frac{\partial c}{\partial t} + (u_j + u^s e_j^g)\frac{\partial c}{\partial x_j} = \frac{1}{ScRe}\frac{\partial^2 c}{\partial x_j \partial x_j}. \tag{4}$$

In the Eq.(4) the mass is transported taking into account the flow and settling velocities. The concentration field is expressed by c and the $Sc = \tilde{\nu}/\tilde{k}$ is the Schmidt number which is the relation between the viscous ($\tilde{\nu}$) and mass diffusivity ($\tilde{k}$). Sc is setted as one for all simulations to reduce computational costs.

Table 1: Summary of the simulation parameters.

	Re	$L_{1_s}, L_{2_s}, L_{3_s}$	n_1, n_2, n_3	Δt
Case 1	1000	1, 2, 2	1201, 193, 1201	4×10^{-4}
Case 2	1000	2, 2, 1	1201, 193, 1201	4×10^{-4}
Case 1	5000	1, 2, 2	1201, 289, 1201	5×10^{-4}
Case 2	5000	2, 2, 1	1201, 289, 1201	5×10^{-4}

The open source code `Incompact3d`[1] is used to solve these equations in a structured Cartesian mesh. This code is based on sixth-order compact finite differences schemes for spatial discretization and a third order Adams-Bashforth scheme for the time advancement. A spectral method is employed to solve Poisson equation (Laizet and Lamballais (2009)) as well as a 2D decomposition is used for the parallel calculation (details of this strategy can be found in Laizet and Li (2011)). The boundary conditions imposed for the velocity field are free-slip at the vertical walls and no-slip at the top and bottom of the domain. The channel-basin transition is modelled using an immersed boundary method proposed by Parnaudeau et al. (2008) which satisfy no-slip and no-flux boundary conditions. Regarding to the concentration field, no-flux boundary conditions at the top and vertical walls are adopted, whereas at the bottom an advective equation is used to mimic the particle deposition and it is expressed as

$$\frac{\partial c}{\partial t} + u^s e_2^g \frac{\partial c}{\partial x_2} = 0, \tag{5}$$

this condition allows the particles to leave the domain when they touch the bottom. At the initial condition a weak perturbation is added to the velocity field, around the interface where the gate is localized, aiming to reproduce de disturbance generated by releasing of the mixture .

3. NUMERICAL RESULTS

The four high-fidelity simulations presented here are carried out in a computational domain ($L_1 \times L_2 \times L_3$) = ($12 \times 2 \times 12$), discretized by ($n_1 \times n_2 \times n_3$) mesh nodes for a settling velocity $u^s = 0.02$. We use two Reynolds number and two initial sub-volume aspect ratio to differentiate the simulations. The list of parameters are shown in Tab. 1.

Figure 2 shows snapshots of the concentration field at the same time (t = 10), where it is possible to see the spanwise and streamwise expansion of the current. The spreading of the current has a tongue shape and it is evident the influence of the Reynolds number over the flow front evolution for equal sub-volume aspect ratio. While Re = 1000 shows a smooth propagation with a good symmetry in the spanwise direction, the simulations with Re = 5000 develop intense turbulence in their head and body, and the lobe and cleft structures at the front of the current are present. At this time we can see very little material inside the reservoir in the Case 1 simulations, unlike Case 2 that presents considerable amount of concentration for both Reynolds numbers. This fact reflects on the front evolution of the current, where a wider supply channel contributes to a greater spreading of the current over the bottom of the domain.

We plot the current front position as a function of time in Fig. 3 to better view the influence of the Reynold and the aspect ratio. Comparisons of the front evolution along the L_1 direction (x_{1f}) are established with that results presented by Bonnecaze et al. (1995) and Zgheib et al. (2015c) in order to validate our results. A good agreement with the axysimmetric experimental data (Bonnecaze et al., 1995) can be seen even though their Reynols number is 6100. The comparison with the axysimmetric simulation data (Zgheib et al., 2015c) shows a small difference after $t \approx 9$, probably because its low Reynolds number equal to 3536. Until $t \approx 4$ we can see the same constant front velocity in all results, regardless the Reynolds number, symmetry or initial reservoir. This behaviour indicates that the current evolution it is not affected by the intensity (related to Re) nor the particle sedimentation. After $t \approx 4$, our curves deviate from constant velocity, where x_{1f} Case 1 is greater than Case 2 and Re = 5000 prevails over Re = 1000 considering the same Case. In the Fig. 3 it is also shown the current front evolution in the spanwise direction (x_{3f}) along the positive L_3 axis, where x_{3f} is very similar for all simulations up to $t \approx 4$. This lateral spreading is mainly ruled by the Reynolds once Re = 5000 reaches longer distances than Re = 1000. Comparing Case 1 and Case 2 we can not highlight differences for Re = 1000, but for Re = 5000 the Case 1 starts to deviates from Case 2 after $t \approx 10$.

The streamwise front velocity of the current (u_{1f}) is present in Fig. 4 for all simulations. Cylindrical initial reservoirs spreads in four different phases (Cantero et al., 2007a). At the first times the current accelerates up to $t \approx 0.8$ with $u_{1f} \sim t^{0.75}$. After this short acceleration period, the current enters in the slumping phase which its velocity is almost constant with $u_{1f} \sim t^0$. This phase reaches $t \approx 5$ and it is associated with the reservoir empting, then it passes through a brief inertial phase where the buoyancy forces are balanced by the inertial forces with $u_{1f} \sim t^{-0.5}$. Finally the current

[1]This code is available for download at www.incompact3d.com

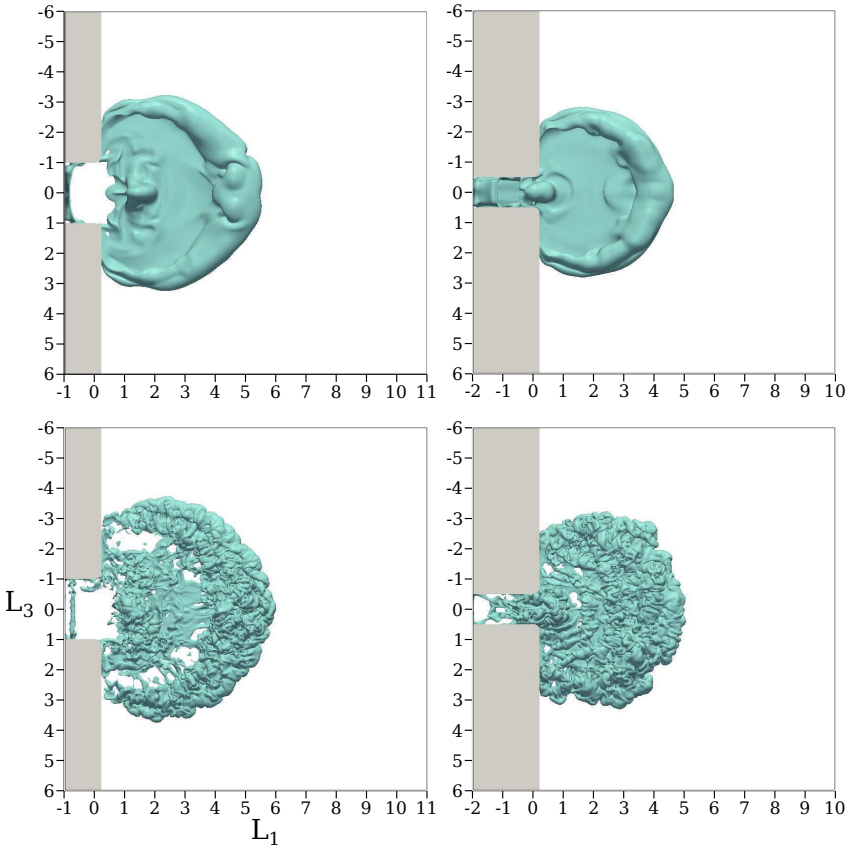

Figure 2: Concentration field at t = 10 for Case 1 (left) and Case 2 (right) with Re = 1000 (top) and Re = 5000 (bottom). The snapshots are taken for an iso-value c = 0.08.

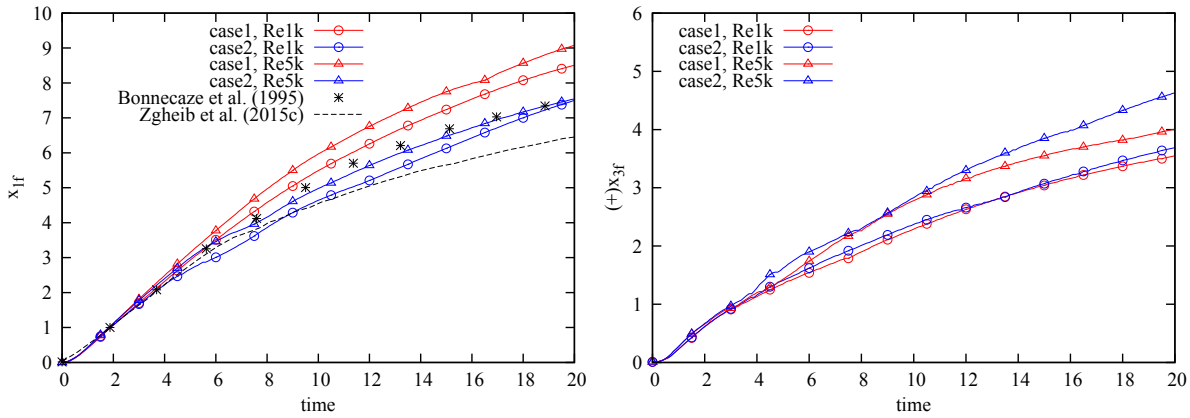

Figure 3: Evolution of the current front position as a function of time. Left shows the evolution in the L_1 direction (x_{1f}), taken in a center plan at x_3 = 0 and compared with experimental result of Bonnecaze et al. (1995) and sumulation of Zgheib et al. (2015c). Right shows the relative front position in the spanwise direction (x_{3f}) starting from the lateral vertical wall of the channel. The plotted values for (x_{3f}) were taken in the positive side of the L_3 axis.

enters in the viscous phase when the viscous effects become important for the flow decelerating with velocity u_{1f} is proportional to $t^{-1.5}$.

A way to visualize the intensity of the flow turbulence is using the Q-criterion, which is defined by $Q = \frac{1}{2}\left(\Omega_{ij}\Omega_{ij} - S_{ij}S_{ij}\right)$, where Ω_{ij} is the rotation rate tensor and S_{ij} is the strain rate tensor (Dubief and Delcayre, 2010). Figure 5 shows the time evolution of the positive Q-criterion for the Re = 5000 Case 1 and t = 8, 12 and 20. The positive Q depicts regions where the fluid rotation overcomes the fluid shearing, which forms coherent structures like "worms". At t = 8 there is intense turbulence in the entire current although it is possible distinguish a portion, located in the head of the current, where this intensity is more evident. At subsequent times the current is subdivided between two regions of intense turbulence, where the first is located approximately at half of the x_{1f} and the second one is in the frontal portion of the current, for both t = 12 and t = 20. It seems that the turbulent intensity at t = 20 decreases because we have less coherent structures, probably

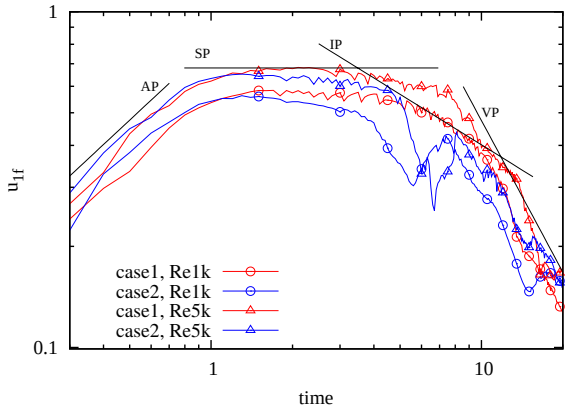

Figure 4: Time evolution of the stramwise current front velocity in log-log scale. The black lines depict the transition phases of spreading. AP: acceleration phase; SP: slumping phase; IP: inertial phase; VP: viscous phase.

due the loss of potential energy of the current by the sedimentation process.

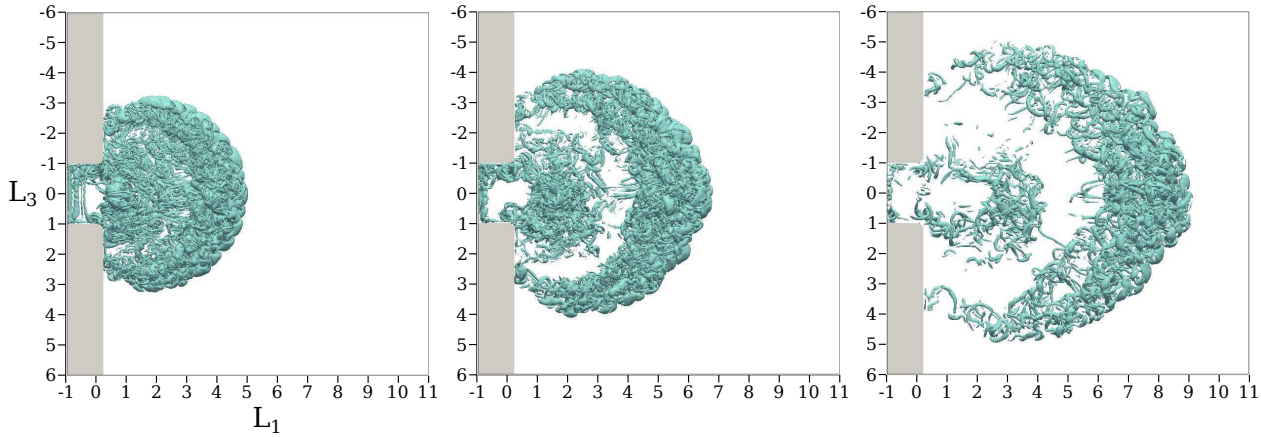

Figure 5: Iso-surfaces of the Q-criterion for an iso-value Q = 1. The pictures are taken for Re = 5000 Case 1 and t = 8, 12 and 20 from left to right.

The sedimentation process forms layers at the bottom of the domain with different heights and it can be seen in the Fig. 6 using isolines for some values. The deposit map is obtained by time integration of the concentration at the bottom as fallow

$$D(x_1, x_3, t) = \int_0^t u^s c_w(x_1, x_3, t) dt, \tag{6}$$

where c_w is the instantaneous concentration at the bottom wall. The greater thickness are found in the Case 2 for both Reynolds 1000 and 5000 in a region near to the end of the channel and more investigations are needed to correctly understand such behaviour. In these cases, the largest amount of deposited particles are concentrated mainly in the center of the current, inside an imaginary circle with radius about 1.8, as depicted in the Fig. 6. On the other hand, the Case 1 simulations show the particles are reaching longer distances from the end of the channel, which reflects in lower heights of the deposit layer if we compare with Case 2. Another important aspect is the dendritic shape of the deposit map for Re = 5000.

4. CONCLUSIONS

We have presented here Direct Numerical Simulations for non-channelized non-axisymmetric particle-laden gravity currents with the purpose of understand how the Reynolds number and the aspect ratio of the reservoir of the mixture particle-fluid affect the dynamics of such flows. The first implication observed is that wider channels ($L_{3s} > L_{1s}$) facilitate the emptying, which contributes for the particle spreading into the basin, and the Reynolds number have a significant effect on the turbulence and the symmetry of the current. The front evolution in the L_1 direction (x_{1f}) has presented, approximately, the same constant velocity up to $t \approx 4$, regardless Re or the aspect ratio of the reservoir. After this time, the Case 1 simulations for both Re = 1000 and Re = 5000 advance faster than the Case 2, which means that

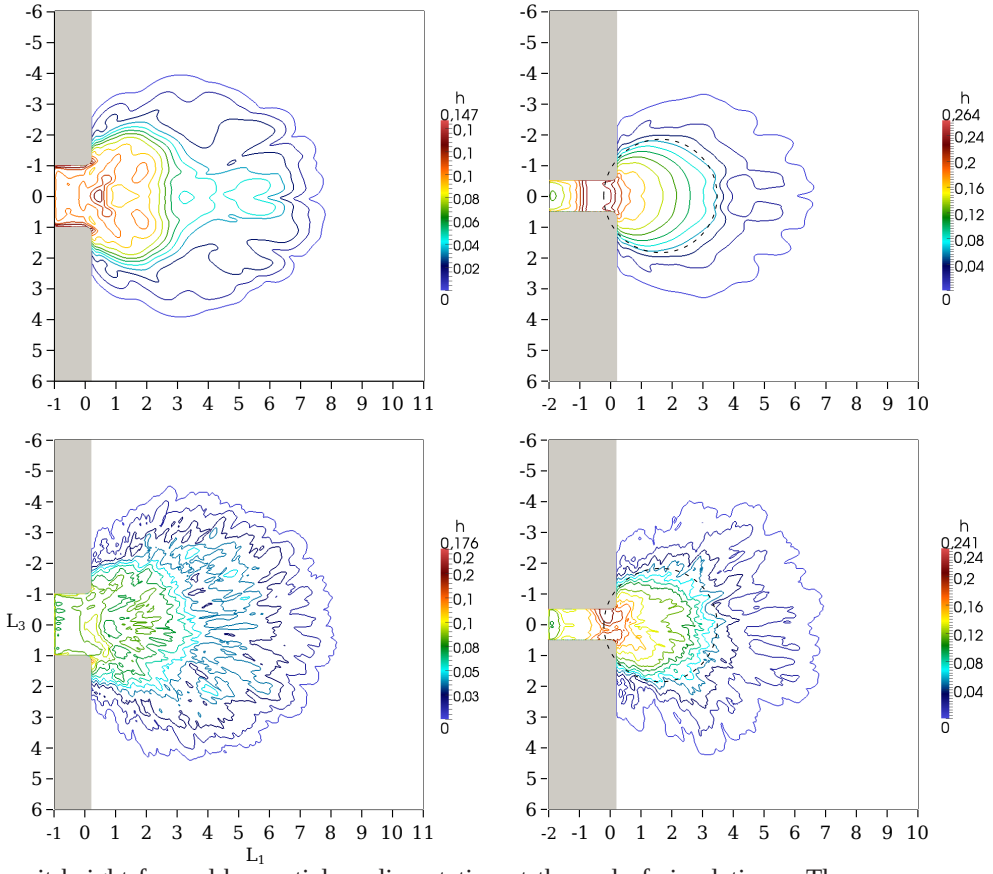

Figure 6: Deposit height formed by particle sedimentation at the end of simulations. The curves are scales with the respective maximum final deposit height. Case 1 are the pictures in the left and Case 2 in the right. Re = 1000 in at the top and Re = 5000 in at the bottom.

the important parameter for longitudinal advancement are the dimensions of the reservoir. On the other hand, the results obtained for the lateral evolution (x_{3f}) have shown the opposite, where the spreading is mainly ruled by Reynold. The deposit map shows that the higher Reynolds produces a dendritic spreading of the current in the Case 1 and 2. When $L_{1s} > L_{3s}$ (Case 2), considerable amount of particle accumulate in a regions near to the end of the channel and inside the channel.

5. ACKNOWLEDGEMENTS

The authors are grateful to Petrobras for supporting this research. This work was achieved in cooperation with Hewlett-Packard Brasil Ltda. using incentives of Brazilian Informatics Law. All simulations have been carried out at the Pontifical Catholic University of Rio Grande do Sul (PUCRS) High Performance Computing Facility LAD.

6. REFERENCES

Blanchette, F., Piche, V., Meiburg, E. and Strauss, M., 2006, "Evaluation of a simplified approach for simulating gravity currents over slopes of varying angles", Computers and fluids, Vol. 35, pp. 492-500.

Bonnecaze, R. T., Hallworth, M. A. and Lister, J. R., 1995, "Axysimmetric particle-driven gravity currents", J. Fluid Mech., Vol. 295, pp. 93-121.

Cantero, M. I., Balachandar, S., Garcia, M. H., Ferry, J. P., 2006, "Direct Numerical Simulations of Planar and Cylindrical Density Currents", J. of Applied Mechanics, Vol. 73, pp. 923-930.

Cantero, M. I., Balachandar, S., Garcia, M. H., 2007, "High-resolution simulations of cylindrical density currents", J. Fluid Mech., Vol. 590, pp. 437-469.

Cantero, M. I., Lee, J. R., Balachandar, S., Garcia, M. H., 2007, "On the front velocity of gravity currents", J. Fluid Mech., Vol. 586, pp. 1-39.

Dubief, Y. and Delcayre, F., 2000, "On coherent-vortex identification in turbulence", Journal of Turbulence, Vol. 1, pp. 22.

Espath, L. F. R., Pinto L. C., Laizet, S. and Silvestrini J. H., 2014, "Two- and three-dimensional direct numerical simula-

tion of particle-laden gravity currents", Computers and Geosciences, Vol. 63, pp. 9-16.
Espath, L. F. R., Pinto L. C., Laizet, S. and Silvestrini J. H., 2015, "High-fidelity simulations of the lobe-and-cleft structures and the deposition map in particle-driven gravity currents", Physics of Fluids, Vol. 27, pp. 056604.
Gladstone, C., Phillips, J. and Sparks, R., 1998, "Experiments on bidisperse, constant-volume gravity currents: propagation and sediment deposition", Sedimentology, Vol. 45, pp. 833-843.
Gray, T. E., Alexander, J. and Leeder, M. R., 2005, "Quantifying velocity and turbulence structure in depositing sustained turbidity currents across breaks in slope", Sedimentology, Vol. 52, pp. 467-488.
Julien, P. Y., 1998, "Erosion and Sedimentation", Cambridge University Press, 280 p.
Kneller, B. and Buckee, C., 2000, "The structure and fluid mechanics of turbidity currents: a review of some recent studies and their geological implications", Sedimentology, Vol. 47, pp. 62-94.
Laizet, S. and Lamballais, E., 2009, "High-order compact schemes for incompressible flows: A simple and efficient method with quasi-spectral accuracy", Journal of Computational Physics, Vol. 228, pp. 5989-6015.
Laizet, S. and Li, N., 2011, "A powerful tool to tackle turbulence problems with up to $O(10^5)$ computational cores", International Journal for Numerical Methods in Fluids, Vol. 67, pp. 1735-1757.
Meiburg, E. and Kneller, B., 2010, "Turbidity currents and their deposits", Annu. Rev. Fluid Mech., Vol. 42, pp. 135-156.
Necker, F., Härtel, C., Kleiser, L. and Meiburg, E., 2002, "High-resolution simulations of particle-driven gravity currents", J. Multiphase Flow, Vol. 28, pp. 279-300.
Necker, F., Härtel, C., Kleiser, L. and Meiburg, E., 2005, "Mixing and dissipation in particle-driven gravity currents", J. Fluid Mech., Vol. 545, pp. 339-372.
Parnandeau, P., Carlier, J., Heitz, D. and Lamballais, E., 2008, "Experimental and numerical studies of the flow over a circular cylinder at Reynolds number 3900", Phys. Fluids, Vol. 20, 085101.
Rooij, F. D. and Dalziel, S. B., 2001, "Time-and space-resolved measurements of deposition under turbidity currents", Special publication of the international association of Sedimentologists, Vol. 31, pp. 207-215.
Ungarish, M., 2006, "Energy balances for propagating gravity currents: homogeneous and stratified ambients", J. Fluid Mech, Vol. 565, pp. 363-380.
Zgheib, N., Bonometti, T., Balachandar, S., 2014, "Long-lasting effect on initial configuration in gravitational spreading of material fronts", Theor. Comput. Fluid Dyn., Vol. 28, pp. 521-529.
Zgheib, N., Bonometti, T. Balachandar, S., 2015a, "Propagation and deposition of non-circular finite release particle-laden currents", Physics of Fluids, Vol. 27, pp. 086604.
Zgheib, N., Bonometti, T. Balachandar, S., 2015b, "Dynamics of non-circular finite-release gravity currents", J. Fluid Mech., Vol. 783, pp. 344-378.
Zgheib, N., Bonometti, T. Balachandar, S., 2015c, "Direct numerical simulation of cylindrical particle-laden gravity currents", Computers and Fluids, Vol. 123, pp. 23-31.

7. RESPONSIBILITY NOTICE

The authors are the only responsible for the printed material included in this paper.